Binding of trifluoperazine to apocalmodulin revealed by a combination of small-angle X-ray scattering and nuclear magnetic resonance

Norio Matsushima,[a]***** **Nobuhiro Hayashi,**[b] **Noriko Watanabe,**[c] **Yuji Jinbo**[c] **and Yoshinobu Izumi**[c]

[a]Department of Biophysics, School of Health Sciences, Sapporo Medical University, Sapporo, Hokkaido 060-8556, Japan, [b]Division of Biomedical Polymer Science, Institute for Comprehensive Medical Science, Fujita Health University, Toyoake, Aichi 470-1192, Japan, and [c]Graduate School of Science and Engineering, Yamagata University, Yonezawa, Yamagata 992-8510, Japan. Correspondence e-mail: matusima@sapmed.ac.jp

Small-angle X-ray scattering (SAXS) and nuclear magnetic resonance (NMR) studies were performed to investigate the binding of trifluoperazine (TFP) to Ca^{2+}-free calmodulin (apoCaM) with N- and C-terminal globular domains connected by a linker. The SAXS and NMR measurements were taken throughout the titration of TFP. The SAXS analyses indicate that the binding of TFP induces structural changes from a dumbbell shape to a compact globular shape in solution. The formation of the complete globular structure requires 5.0 added equivalents of TFP. An analysis of NMR chemical-shift changes indicates that the C-terminal domain of apoCaM is involved in the binding of TFP. The SAXS and NMR data reflect the high structural flexibility of apoCaM.

1. Introduction

Calmodulin (CaM) is a ubiquitous, EF-hand Ca^{2+}-binding protein of 148 residues with N- and C-terminal globular domains connected by a flexible linker. Each of the two domains possesses two helix–loop–helix Ca^{2+}-binding motifs referred to as EF hands and the protein binds a total of four Ca^{2+} ions. Helices $\alpha A/\alpha B$ and $\alpha C/\alpha D$ make up the N-domain EF hands I and II, respectively, whereas helices $\alpha E/\alpha F$ and $\alpha G/\alpha H$ make up the C-domain EF hands III and IV, respectively. A comparison of the structure of Ca^{2+}-free CaM (apoCaM) and Ca^{2+}-bound CaM (Ca^{2+}CaM) reveals that the two globular domains rotate outward on Ca^{2+} binding, increasing the distance between them (Babu et al., 1985; Chattopadhyaya et al., 1992; Wilson & Brunger, 2000; Kuboniwa et al., 1995; Zhang et al., 1995). This changes the overall conformation of the protein from the extended structure of apoCaM to the more extended characteristic dumbbell shape of Ca^{2+}CaM. This increase in radius of gyration (R_g) of the protein was observed in small-angle X-ray scattering (SAXS) studies (Seaton et al., 1985; Heidorn et al., 1989; Matsushima et al., 1989, 2000).

CaM regulates numerous target CaM-binding proteins that are functionally and structurally diverse. The first target proteins were identified in a Ca^{2+}-dependent manner, while other target proteins have been identified even in the absence of Ca^{2+}. An IQ or IQ-like domain often mediates Ca^{2+}-independent CaM binding (reviewed in Jurado et al., 1999; Bähler & Rhoads, 2002). Ca^{2+}-dependent target proteins primarily contain domains that can be classified into motifs based upon variations on the basic amphiphilic α-helix domain involving conserved hydrophobic residues at positions 1–10, 1–14 or 1–16 (reviewed in Rhoads & Friedberg, 1997; Ikura et al., 2002; Yamniuk & Vogel, 2004). SAXS measurements of Ca^{2+}CaM with an amphiphilic peptide such as mastoparan or mellitin and a peptide from myosin light chain kinase (MLCK) showed large conformational changes of Ca^{2+}CaM (Matsushima et al., 1989; Heidorn et al.,

1989; Kataoka et al., 1989). We proposed that Ca^{2+}CaM complexed with mastoparan adopts a compact globular shape by bending of the domain linker (Matsushima et al., 1989). This was confirmed by crystallographic and nuclear magnetic resonance (NMR) studies on various target Ca^{2+}CaM-binding proteins including MLCK, CaM-dependent protein kinase (CaMK) and myristoylated alanine-rich C-kinase substrate (MARCKS) (reviewed in Ikura et al., 2002; Yamniuk & Vogel, 2004; Ikura & Ames, 2006). In contrast, although the interactions of apoCaM have been studied with some target proteins such as neurogranin, cyclic nucleotide phosphodiesterase (PDE), small conductance Ca^{2+}-activated K^+ channel (SK channel), voltage-gated sodium channel, MLCK and myosin V (Cui et al., 2003; Yuan et al., 1999; Mori et al., 2003; Tsvetkov et al., 1999; Hill et al., 2000; Bayley et al., 2003; Akyol et al., 2004; Tang et al., 2003; Jin et al., 2005; Houdusse et al., 2006), structural studies are very rare (Izumi et al., 2001; Schumacher et al., 2004).

Trifluoperazine (TFP) and N-(6-aminohexyl)-5-chloro-1-naphthalenesulfonamide (W-7) have been used extensively as CaM antagonists to study the Ca^{2+}CaM-dependent activation of various enzymes. SAXS studies of Ca^{2+}CaM complexed with TFP and W-7 found that the binding of four TFP or two W-7 molecules to one Ca^{2+}CaM molecule induces structural changes from a dumbbell shape to a compact globular shape (Osawa et al., 1999; Matsushima et al., 2000). Moreover, conformational changes of apoCaM occur in the presence of five TFP molecules per protein molecule (Matsushima et al., 2000). What number of TFP molecules is required to induce the structural changes of apoCaM? What are the structural changes of apoCaM? What is the binding site of TFP on apoCaM? In order to answer these questions, SAXS and NMR measurements were taken for apoCaM upon addition of TFP. The results indicate that TFP molecules bind the C-terminal domain of apoCaM and the binding induces overall conformational changes from a dumbbell shape to a compact globular shape.

conference papers

2. Experimental

2.1. Sample preparation

Recombinant rat CaM was expressed in *Escherichia coli* and purified to homogeneity as described previously (Hayashi *et al.*, 1998). For SAXS measurements, the recombinant was dissolved in tris(hydroxymethyl)aminomethane (Tris) buffer (50 mM Tris–HCl, pH 7.6) containing 120 mM NaCl. The protein concentration was determined by quantitative amino-acid analysis. ApoCaM was dissolved in 3 mM EDTA. The TFP powder was dissolved in water containing $1\%(v/v)$ dimethyl sulfoxide (DMSO) and was added to the apoCaM solution. At every stage, the concentration of DMSO was kept at 1.0%. For SAXS measurements, a series of solutions of apoCaM complexed with 0.0, 1.0, 2.0, 4.0 and 5.0 equivalents of TFP at four or five protein concentrations in the range 4.0–18.0 mg ml^{-1} were prepared.

2.2. Small-angle X-ray scattering

The measurements were carried out using synchrotron orbital radiation with an instrument for SAXS installed at BL-10C at the Photon Factory, Tsukuba (Ueki *et al.*, 1985). An X-ray wavelength of 1.488 Å was selected. The samples were contained in a mica cell with a volume of 80 μl, and the temperature was maintained at 298.0 ± 0.1 K by circulating water through the sample holder. The modulus of the scattering vector, Q, equal to $(4\pi/\lambda)\sin\theta$, was calibrated by the observation of peaks from dried chicken collagen, where 2θ is the scattering angle and λ is the X-ray wavelength. Scattering data were collected for 250 or 300 s at various protein concentrations.

Two methods of data analysis were used. The first method was that of Guinier (1939), which gives the radius of gyration, R_g. The scattering intensity $I(Q)$ measured as function of Q is given by

$$I(Q) = I(0)\exp[-(1/3)R_g^2Q^2]. \qquad (1)$$

The range of Q used for the Guinier plots was 0.02 to 0.06 Å^{-1}. The second method was that of Kratky (Kratky & Porod, 1949). In a Kratky plot, $Q^2I(Q)$ is plotted against Q to provide information on the structural characteristics (*e.g.* molecular shape) of a chain polymer or a biopolymer (Izumi *et al.*, 2001). Data to $Q = 0.5$ Å^{-1} were used for the analysis.

2.3. Small-angle X-ray scattering intensities of known structures

The structures of apoCaM are available (Kuboniwa *et al.*, 1995; Zhang *et al.*, 1995; Schumacher *et al.*, 2004). The overall scattering intensities, $I(Q)$, can be calculated using Debye's formula (Debye, 1915) containing hydration effects:

$$I(Q) \propto I_{a-a}(Q) - 2I_{a-b}(Q) + I_{b-b}(Q),$$

where

$$I_{a-b}(Q) = \sum\sum f_m^a f_n^b \sin(Qr_{mn})/Qr_{mn}.$$

Here, the superscripts a and b refer to the protein molecule and the solvent, respectively. f_m and f_n are the number of electrons for the mth element and the nth element, respectively. r_{mn} is the distance between the elements m and n (Hubbard *et al.*, 1988). The double summation encompasses all scattering elements in the assemblage. The scattering intensities were used to create Kratky plots which were compared with those of the experimental data obtained here.

2.4. Nuclear magnetic resonance

All of the NMR spectra were measured at 310 K on a Bruker DMX-500 spectrometer (Hayashi *et al.*, 2004). TFP was titrated in aliquots of 0.33 protein equivalents into a uniformly $^{13}C/^{15}N$-labelled sample of the protein. After the addition of each aliquot of TFP, one-dimensional ^1H, two-dimensional ^{15}N–^1H heteronuclear single quantum correlation (HSQC) (Palmer *et al.*, 1991; Kay *et al.*, 1992) spectra were acquired. The sample contained 0.5 mM CaM, 120 mM NaCl, 5 mM EDTA and 50 mM deuterated Tris–HCl (pH 7.5) in 90% H$_2$O and 10% D$_2$O. The resonance assignments were taken by conventional methods using $^{13}C/^{15}N$-labelled CaM. Finally, spectra with 0.0, 1.0, 2.0, 3.0, 4.0 and 5.0 equivalents of TFP to CaM were recorded.

3. Results

3.1. The radius of gyration (R_g) and the Kratky plots

The radii of gyration, R_g, of apoCaM alone and apoCaM with TFP were measured as a function of protein concentration. The values of R_g extrapolated to zero concentration were estimated (Fig. 1). The value of R_g of apoCaM without TFP is comparable with those of apoCaM with 1.0, 2.0 and 4.0 added equivalents of TFP (Fig. 1 and Table 1). All of these values are significantly larger than the R_g value for apoCaM with 5.0 added equivalents of TFP.

Fig. 2 shows the Kratky plots for apoCaM without and with TFP. The Kratky plots for apoCaM without TFP and with 1.0, 2.0 and 4.0 added equivalents of TFP are characterized by the presence of a main peak near $Q = 0.096$ Å^{-1} and a second (shoulder) peak near $Q = 0.14$–0.15 Å^{-1}. The second peak decreases with increasing TFP and finally disappears for apoCaM with 5.0 added equivalents of TFP. Consequently, the Kratky plot for apoCaM with 5.0 added equivalents of TFP shows a single peak at $Q = 0.096$ Å^{-1}.

The scattering intensity was also calculated using two known structures of apoCaM: one is the solution structure of uncomplexed apoCaM (Kuboniwa *et al.*, 1995) and the other is the crystal structure
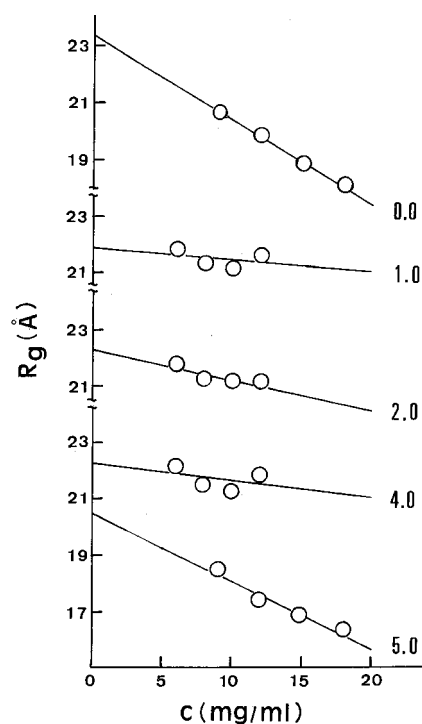

Figure 1
The radius of gyration, R_g, of apoCaM as a function of protein concentration. The five apoCaM samples contain 0.0, 1.0, 2.0, 4.0 and 5.0 added equivalents of TFP.

Table 1
Radius of gyration (R_g) of apocalmodulin (apoCaM) with 0.0, 1.0, 2.0, 4.0 and 5.0 added equivalents of TFP at infinite dilution.

TFP:apoCaM	R_g (Å)
0.0	23.4 ± 0.2
1.0	21.9 ± 0.4
2.0	22.7 ± 0.3
4.0	22.2 ± 0.4
5.0	20.5 ± 0.3

of apoCaM complexed with the SK channel gating domain (Schumacher *et al.*, 2004). The Kratky plot for the solution structure is characterized by two peaks at $Q = 0.1$ and 0.16 Å^{-1} (Fig. 3). This behaviour is close to that of apoCaM without TFP (Figs. 2 and 3). Similarly, the Kratky plot for the crystal structure, which shows a single peak at $Q = 0.1$ Å^{-1}, is consistent with that of the 1:5 apoCaM–TFP complex (Figs. 2 and 3).

3.2. NMR spectral changes

The NMR spectral changes in the $^{15}N-^1H$ HSQC spectra of uniformly $^{13}C/^{15}N$-labelled apoCaM were monitored upon addition of TFP. Fig. 4 shows selected portions of the spectra for apoCaM:TFP molar ratios from 1:0 to 1:5. Most of the HSQC peaks in each of the two CaM domains (Ala1 to Lys148) were gradually shifted with little change in their intensities, indicating that the conformational exchange rate between TFP in the bound state and in the unbound state is fast on the NMR timescale. The NMR signal peaks originating from N-terminal domain residues showed little change compared to some of those in the C-terminal domain. In contrast, the signals from
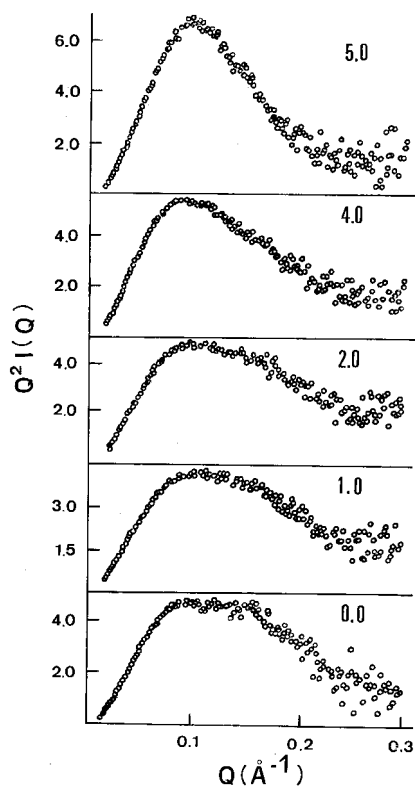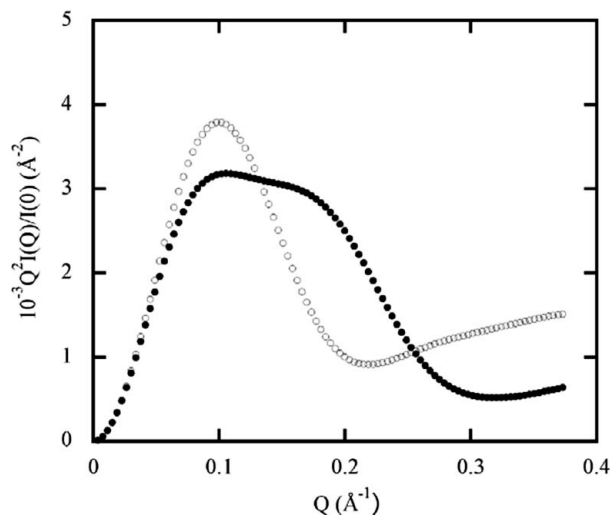

Figure 3
Kratky plots for apoCaM calculated using the theoretical intensities of two known structures. Open circles: apoCaM complexed with the SK channel gating domain (1QX7); filled circles: uncomplexed apoCaM (1CFC).

eleven residues in the C-terminal domain showed larger chemical shifts (Fig. 4). These residues are Gly113, Asp131, Asn137, Tyr138, Glu139, Glu140, Phe141, Gln143, Met145, Thr146 and Ala147. Interestingly, the chemical shift of Asn137 showed a marked change with 2.0 added equivalents of TFP.

4. Discussion

4.1. The structure of the apoCaM–TFP complexes

Comparison of the Kratky plots for the experimental data and the theoretical calculation demonstrates that the overall structure of apoCaM without TFP is almost the same as the solution structures revealed by NMR measurements (Figs. 5a and 5b) (Kuboniwa *et al.*, 1995; Zhang *et al.*, 1995), as expected. That is, the solution structures adopt a dumbbell shape, although it is different from the more extended characteristic dumbbell shape of Ca^{2+}CaM. In contrast, the

Figure 2
Kratky plots for apoCaM calculated using the intensities of the SAXS measurements. The five apoCaM samples contain 0.0, 1.0, 2.0, 4.0 and 5.0 added equivalents of TFP. The protein concentration of the samples is 12.0 mg ml^{-1}. The intensities are on an arbitrary scale.
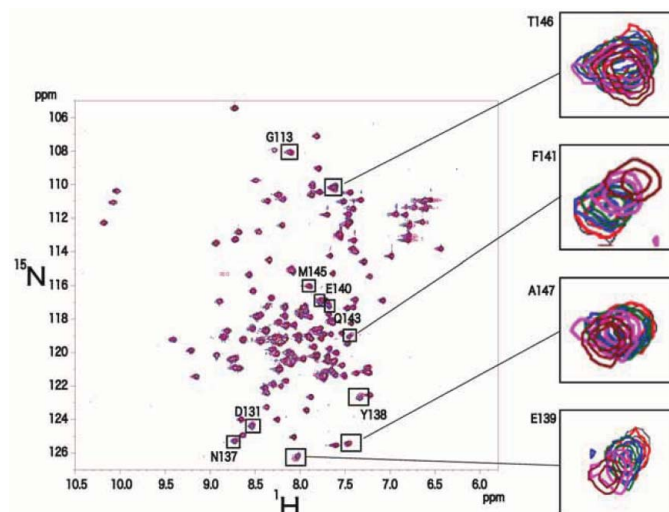

Figure 4
NMR spectral changes for apoCaM amide groups upon TFP binding. The whole region is shown. Some well isolated regions are shown by the expansions. The spectra of apoCaM in the presence of 0.0, 1.0, 2.0, 3.0, 4.0 and 5.0 added equivalents of TFP are indicated by brown, pink, green, blue, red and black, respectively.
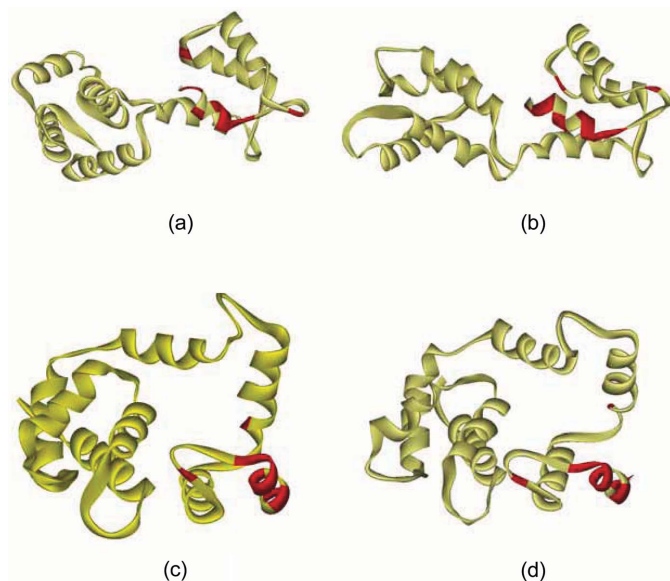
Figure 5
Known structures of apoCaM prepared using *DS ViewerPro*. (a) The crystal structure of apoCaM complexed with the SK channel gating domain (1QX7) (Schumacher *et al.*, 2004); (b) the crystal structure of apoCaM in a dimer (1QX5) (Schumacher *et al.*, 2004); (c) the solution structure of apoCaM (1CFC) (Kuboniwa *et al.*, 1995); (d) the solution structure of apoCaM (1MDO) (Zhang *et al.*, 1995). The residues whose chemical shifts changed upon forming the apoCaM–TFP complex observed here are indicated in red.

1:5 apoCaM–TFP complex adopts a compact globular structure which is similar to apoCaM complexed with the SK channel gating domain (Fig. 5c) (Schumacher *et al.*, 2004). These present results correspond to the previous analysis of the pair distance distribution; uncomplexed apoCaM adopts a dumbbell shape and the 1:5 apoCaM–TFP complex adopts an ellipsoid shape (Matsushima *et al.*, 2000).

The Kratky plots and the R_g values indicate that 5.0 added equivalents of TFP induce a complete compact globular shape of apoCaM. What are the apoCaM structures with 1.0, 2.0 and 4.0 added equivalents of TFP? There are two possibilities. One is that the apoCaM structures consist of a mixture of the compact globular structure (of the 1:5 apoCaM–TFP complex) and the dumbbell structure (of apoCaM without TFP) in solution. The other is an intermediate structure between these two extreme structures. Finally, it can be concluded that the formation of the complete globular structure requires 5.0 added equivalents of TFP.

4.2. Structural flexibility of apoCaM

The present results demonstrate that the binding to apoCaM of TFP induces conformational changes from a dumbbell shape to a globular shape. In contrast, the interaction of apoCaM with a peptide having a 1–5–8–14 motif in human Ca^{2+}/CaM-dependent protein kinase IV appears to induce an increase in the R_g value and the apoCaM molecule keeps a dumbbell shape (Izumi *et al.*, 2001). In addition, the IQ motif from neuromodulin, IQASFR-GHITRKKLKGEK, does not bring about a change in the R_g value (data not shown), indicating that the protein keeps a dumbbell shape. The dumbbell structure has been observed in the crystal structure of apoCaM complexed with the first two IQ motifs of myosin V (Houdusse *et al.*, 2006). These two patterns in the molecular recognition infer that the flexible linker connecting the N- and C-terminal globular domains is influenced by the binding of TFP/target peptides to the C-terminal domain (Izumi *et al.*, 2001).

The present NMR data showed no interdomain NOE in apoCaM complexed with TFP, suggesting that the relative orientation of the two domains is not always fixed due to a conformational change between various orientations, as observed in Ca^{2+}/CaM complexed with W-7 (Osawa *et al.*, 1999). The lack of an NOE is consistent with the idea that the interdomain interaction is unstable and involves a rapid exchange between the associated and dissociated states. The SAXS data indicate that the time- and spatially averaged shape of the apoCaM–TFP complex is a compact globular one. These NMR and SAXS observations are likely to be explained by the flexible linker of apoCaM.

Two solution structures and one crystal structure of apoCaM without a ligand are available. The two solution structures adopt a dumbbell shape, although the C-terminal domain has a substantially different conformation (Figs. 5a and 5b) (Zhang *et al.*, 1995; Kuboniwa *et al.*, 1995). On the other hand, the crystal structure forms a domain-swapped dimer between the C-terminal domain subunits in which the intramolecular EF-hand pairing between EF III and IV is destroyed, and then adopts a compact globular structure (Fig. 5d) (Schumacher *et al.*, 2004). These observations reflect the structural flexibility of apoCaM including the C-terminal domain in addition to the flexible linker.

4.3. TFP binding on the C-terminal domain of apoCaM

The present results indicated that the chemical-shift changes occurred at the 11 residues Gly113, Asp131, Asn137, Tyr138, Glu139, Glu140, Phe141, Gln143, Met145, Thr146 and Ala147. The N-terminal domain with four α-helices (αA, residues 6–18; αB, residues 29–39; αC, residues 44–55; and αD, residues 65–76) encompasses two EF hands I and II (Zhang *et al.*, 1995). The N-terminal domain is connected to the C-terminal domain by residues 77–80. The C-terminal domain, like the N-terminal domain, contains fours α-helices (αE, residues 81–91; αF, residues 102–111; αG, residues 118–127; and αH, residues 138–146) that encompass two EF hands III and IV. The Ca^{2+}-binding loops are comprised of residues 20–31 and 56–67 in the N-terminal domain and residues 93–104 and 129–140 in the C-terminal domain. Thus, Gly113 is located between αF and αG, and Asp131 and Asn137 in the Ca^{2+}-binding loops. The remaining residues – Tyr138, Glu139, Glu140, Phe141, Gln143, Met145 and Thr146 – are located at αH and Ala147 at the C-terminus. It is concluded that these eleven residues are located only at the C-terminal domain (Fig. 5).

There is increasing evidence that the C-terminal domain of apoCaM interacts with various peptides from target proteins (Cui *et al.*, 2003; Yuan *et al.*, 1999; Schumacher *et al.*, 2004; Mori *et al.*, 2003; Tsvetkov *et al.*, 1999; Hill *et al.*, 2000; Izumi *et al.*, 2001; Houdusse *et al.*, 2006). The crystal structure of the apoCaM/SK channel gating domain complex revealed that the Tyr435 side chain in the CaM-binding domain makes van der Waals contact with residues in αE and αH (Schumacher *et al.*, 2004). The NMR measurement of an IQ motif of neurogranin, AAAKIQASFRGHMARKKIKSG, observed chemical-shift changes in both the N- and C-terminal domains (Cui *et al.*, 2003). The analysis indicated that the main interaction and conformational changes occurred in the C-terminal domain and αH may be involved in the binding process. Furthermore, the crystal structure of an apoCaM/myosin V IQ motifs complex revealed that the C-terminal domain interacts with the two IQ motifs (Houdusse *et al.*, 2006). These three observations and the present result strongly suggest that the C-terminal domain plays a crucial role in interactions between apoCaM and TFP/target proteins.

The eleven residues on the C-terminal domain interact with TFP, as noted. Are five molecules of TFP per protein necessary for the

interaction? Their chemical shifts are observable even with 1.0 added equivalents of TFP. However, 5.0 added equivalents of TFP are required for the formation of the complete globular structure of apoCaM. These observations suggest that its formation is due to not only van der Waals contacts but also electrostatic interactions and entropy effects.

5. Conclusion

A combination of SAXS and NMR is useful in understanding protein–ligand interactions. The C-terminal domain of apoCaM interacts with TFP molecules. The binding of TFP to apoCaM induced a structural change from a dumbbell shape to a compact globular shape. The complete globular structure required 5.0 added equivalents of TFP. The SAXS and NMR data reflect the high structural flexibility of apoCaM including the flexible linker and the C-terminal domain.

References

Akyol, Z., Bartos, J. A., Merrill, M. A., Faga, L. A., Jaren, O. R., Shea, M. A. & Hell, J. W. (2004). *J. Biol. Chem.* **279**, 2166–2175.

Babu, Y. S., Sack, J. S., Greenhough, T. J., Bugg, C. E., Means, A. R. & Cook, W. J. (1985). *Nature (London)*, **315**, 37–40.

Bähler, M. & Rhoads, A. (2002). *FEBS Lett.* **513**, 107–113.

Bayley, P., Martin, S., Browne, P. & Royer, C. (2003). *Eur. Biophys. J.* **32**, 122–127.

Chattopadhyaya, R., Meador, W. E., Means, A. R. & Quiocho, F. A. (1992). *J. Mol. Biol.* **228**, 1177–1192.

Cui, Y., Wen, J., Hung Sze, K., Man, D., Lin, D., Liu, M. & Zhu, G. (2003). *Anal. Biochem.* **315**, 175–182.

Debye, P. (1915). *Ann. Phys.* **46**, 809–823.

Guinier, A. (1939). *Ann. Phys.* **12**, 166–237.

Hayashi, N., Matsubara, M., Takasaki, A., Titani, K. & Taniguchi, H. (1998). *Protein Expr. Purif.* **12**, 25–28.

Hayashi, N., Nakagawa, C., Ito, Y., Takasaki, A., Jinbo, Y., Yamakawa, Y., Titani, K., Hashimoto, K., Izumi, Y. & Matsushima, N. (2004). *J. Mol. Biol.* **338**, 169–180.

Heidorn, D. B., Seeger, P. A., Rokop, S. E., Blumenthal, D. K., Means, A. R., Crespi, H. & Trewhella, J. (1989). *Biochemistry*, **28**, 6757–6764.

Hill, T. J., Lafitte, D., Wallace, J. I., Cooper, H. J., Tsvetkov, P. O. & Derrick, P. J. (2000). *Biochemistry* **39**, 7284–7290.

Houdusse, A., Gaucher, J. F., Krementsova, E., Mui, S., Trybus, K. M. & Cohen, C. (2006). *Proc. Natl Acad. Sci. USA*, **103**, 19326–19331.

Hubbard S. R., Hodgson, K. O. & Doniach, S. (1988). *J. Biol. Chem.* **263**, 4151–4158.

Ikura, M. & Ames, J. B. (2006). *Proc. Natl Acad. Sci. USA*, **103**, 1159–1164.

Ikura, M., Osawa, M. & Ames, J. B. (2002). *Bioessays*, **24**, 625–636.

Izumi, Y., Kuwamoto, S., Jinbo, Y. & Yoshino, H. (2001). *FEBS Lett.* **495**, 126–130.

Jin, H., Sha, D., Wei, J., Davis, K. M., Wu, H., Jin, Y. & Wu, J. Y. (2005). *J. Neurochem.* **92**, 739–748.

Jurado, L. A., Chockalingam, P. S. & Jarrett, H. W. (1999). *Physiol. Rev.* **79**, 661–682.

Kataoka, M., Head, J. F., Seaton, B. A. & Engelman, D. M. (1989). *Proc. Natl Acad. Sci. USA*, **86**, 6944–6948.

Kay, L. E., Keifer, P. & Saarinen, T. (1992). *J. Am. Chem. Soc.* **114**, 10663–10665.

Kratky, O. & Porod, G. (1949). *Recl Trav. Chim. Pays-Bas*, **68**, 106–122.

Kuboniwa, H., Tjandra, N., Grzesiek, S., Ren, H., Klee, C. B. & Bax, A. (1995). *Nature Struct. Biol.* **2**, 768–776.

Matsushima, N., Hayashi, N., Jinbo, Y. & Izumi, Y. (2000). *Biochem. J.* **347**, 211–215.

Matsushima, N., Izumi, Y., Matsuo, T., Yoshino, H., Ueki, T. & Miyake, Y. (1989). *J. Biochem.* **105**, 883–887.

Mori, M., Konno, T., Morii, T., Nagayama, K. & Imoto, K. (2003). *Biochem. Biophys. Res. Commun.* **307**, 290–296.

Osawa, M., Kuwamoto, S., Izumi, Y., Yap, K. L., Ikura, M., Shibanuma, T., Yokokura, H., Hidaka, H. & Matsushima, N. (1999). *FEBS Lett.* **442**, 173–177.

Palmer, A. G. III, Cavanagh, J., Wright, P. E. & Rance, M. (1991). *J. Magn. Reson.* **93**, 151–170.

Rhoads, A. R. & Friedberg, F. (1997). *FASEB J.* **11**, 331–340.

Schumacher, M. A., Crum, M. & Miller, M. C. (2004). *Structure*, **12**, 849–860.

Seaton, B. A., Head, J. F., Engelman, D. M. & Richards, F. M. (1985). *Biochemistry*, **24**, 6740–6743.

Tang, W., Halling, D. B., Black, D. J., Pate, P., Zhang, J. Z., Pedersen, S., Altschuld, R. A. & Hamilton, S. L. (2003). *Biophys J.* **85**, 1538–1547.

Tsvetkov, P. O., Protasevich, I. I., Gilli, R., Lafitte, D., Lobachov, V. M., Haiech, J., Briand, C. & Makarov, A. A. (1999) *J. Biol. Chem.* **274**, 18161–18164.

Ueki, T., Hiragi, Y., Kataoka, M., Inoko, Y., Amemiya, Y., Izumi, Y., Tagawa, H. & Muroga, Y. (1985). *Biophys. Chem.* **23**, 115–124.

Wilson, M. A. & Brunger, A. T. (2000). *J. Mol. Biol.* **301**, 1237–1256.

Yamniuk, A. P. & Vogel, H. J. (2004). *Mol Biotechnol.* **27**, 33–57.

Yuan, T., Walsh, M. P., Sutherland, C., Fabian, H. & Vogel, H. J. (1999). *Biochemistry*, **38**, 1446–1455.

Zhang, M., Tanaka, T. & Ikura, M. (1995). *Nature Struct. Biol.* **2**, 758–767.